

# Numerical study of the sound fields of temporally-developing supersonic round jets

Pierre Pineau\* and Christophe Bogey†

*Laboratoire de Mécanique des Fluides et d'Acoustique*

*UMR CNRS 5509, École Centrale de Lyon*

*69134, Écully, France*

Numerical simulations of temporally developing isothermal supersonic round jets are performed at a Mach number of 2 in order to investigate sound generation mechanisms in high-speed free-shear flows. Two jets are simulated at diameter-based Reynolds numbers of 3125 and 12500. In the simulations, the compressible Navier-Stokes equations are solved using high-order finite differences on grids extending up to 240 initial jet radii in the axial direction. The temporal development of the turbulent flow and sound field are described by means of instantaneous and statistical representations. The latter include high-order statistics and conditional averages which are computed over four runs using different initial perturbations in the shear layers. It is found that a peak of sound emission occurs respectively before and after the closure of the potential core for the jets of Reynolds numbers 12500 and 3125, respectively. In both cases, the dominant noise generation mechanism is Mach wave radiation. Moreover, skewed shock structures similar to those measured in the acoustic fields of supersonic jets emitting crackle noise are found in the immediate vicinity of the flow at the times of maximum sound emission. The frequency of occurrence of these waves increases with Reynolds number, and their mean directivity slightly differs from that of the global radiated acoustic field. The generation process of these shock structures is investigated using conditional averaging, and they appear to be generated by the supersonic motion of coherent structures inside the jet.

## I. Introduction

In the last decades, there have been significant contributions to the understanding of noise generation mechanisms in supersonic jets. As summarized by Tam,<sup>1</sup> there are three major noise components in supersonic jet noise : turbulent mixing noise, broadband shock noise and screech tones. The latter two are due to shock-turbulence interactions and are only found when the jet is imperfectly expanded at the nozzle exit, whereas the former can be observed even in the absence of a shock cell pattern. When the jet speed is high enough with respect to the ambient speed of sound, Mach waves are generated in the jet shear layers and constitute the major part of the acoustic energy associated with jet mixing noise.<sup>2</sup> These waves are generated by the convection of coherent structures inside the jet at speeds higher than the ambient speed of sound, and they are responsible for the intense peak of sound emission observed at shallow angles from the jet axis in the far field.<sup>1</sup> In the acoustic near field, optical measurements<sup>3-5</sup> as well as numerical simulations of supersonic jets<sup>6,7</sup> show that Mach waves emerge from the shear layers as straight wavefronts oriented in a preferential direction. The angle  $\alpha$  of these wavefronts is related to the convection velocity  $u_c$  of the turbulent structures inside the jet through the relation

$$\cos \alpha = \frac{a_\infty}{u_c}, \quad (1)$$

where  $a_\infty$  is the ambient speed of sound. Oertel<sup>4,8</sup> performed optical measurements in the acoustic field of supersonic jets for a wide range of Mach numbers and temperature ratios, and introduced an empirical

\*PhD student, pierre.pineau@doctorant.ec-lyon.fr.

†CNRS Research Scientist, AIAA Senior Member & Associate Fellow, christophe.bogey@ec-lyon.fr

relation for the convection velocity  $u_c$  of the turbulent structures at the origin of Mach waves. Tam & Burton<sup>9</sup> proposed a description of Mach wave generation using linear stability theory to model the motion of large scale structures inside the jet, and found excellent agreement with the repartition of sound pressure level measured by Troutt & McLaughlin.<sup>10</sup> While linear theory accurately predicts the directivity and the peak Strouhal number of Mach waves,<sup>9,11</sup> it fails to explain the presence of steep, jagged waveforms in the pressure field of high-speed supersonic jets.<sup>12,13</sup> The presence of these shock-like structures is believed to be the cause of crackle noise, an unpleasant perception effect.<sup>12</sup> The mechanism leading to the formation of these weak shock waves is currently unclear. It is known that the sound radiated by supersonic jets exhausting from the nozzles of tactical aircrafts<sup>14</sup> and rocket launchers<sup>15,16</sup> is strong enough to be subject to cumulative nonlinear propagation effects, leading to the gradual formation of shocks. However, the presence of steep waveforms has been found in microphone signals recorded in the far field of model scale supersonic jets even though cumulative nonlinear propagation effects are excluded in these range restricted environments.<sup>17</sup> Moreover, steep wave fronts emerging directly from the turbulent flow have been observed in numerical simulations of supersonic jets<sup>7</sup> and mixing layers.<sup>18–20</sup> These results support the idea that shock waves are generated through a source mechanism located inside the jet, although a comprehensive description of this mechanism remains to be found. Optical measurements by Krothapalli et al.<sup>21</sup> as well as numerical results by Nichols et al.<sup>7</sup> show evidence of steep wavefronts oriented along the Mach wave direction in the near field, which suggests that the source of crackle noise is tightly linked to Mach wave radiation. Moreover, Petitjean et al.<sup>22</sup> and Viswanathan<sup>23</sup> found that a necessary condition for the observation of waves propagating nonlinearly is that the jet convective Mach number  $u_c/a_\infty$  should be higher than unity, which is also an indicator of the presence of Mach waves. More recently, Murray & Lyons<sup>24</sup> measured the near-field orientations of the shock waves and found that they followed a negatively skewed distribution. They inferred that the convection velocities of the events at the origin of these shock waves are positively skewed, suggesting a link between the generation of shock waves and the intermittent occurrence of high convection velocities inside the jet.

In the present study, temporally developing round jets are simulated as model flows to investigate the generation of shock structures in the near field of high-speed perfectly expanded supersonic jets. In the past, the temporal approach has been used to characterize compressibility effects in planar and axisymmetric mixing layers.<sup>25–27</sup> It has also been used, although to a lesser extent, to investigate sound generation in subsonic<sup>28–30</sup> and supersonic<sup>18–20</sup> flows. One major limitation to the use of temporally developing flows as a tool to investigate noise generation is the lack of experimental counterparts to this class of flows, as real-life jets issuing from nozzles have a spatial development. Since the temporal or spatial character of the flow has an impact on the growth of instability waves<sup>31</sup> as well as on the entrainment of ambient air inside the jet,<sup>32</sup> it is not expected here to find perfect quantitative agreement with previous studies of spatially developing flows. Nevertheless, it is likely that a better understanding of the generation of shock waves in temporal flows would allow to shed some light on the source mechanism of crackle noise in realistic supersonic jets.

In this paper, two supersonic isothermal jets are simulated at a Mach number of 2 and at diameter-based Reynolds numbers of 3125 and 12500, respectively. Since a wider range of finer scales are expected to be found in the flow and acoustic fields of the jet at  $Re_D = 12500$ , one objective of this study is to investigate the effects of Reynolds number on the properties of the shock structures radiated by the jets, *e.g.* their strength, directivity, and frequency of occurrence. Moreover, since previous studies have located the source of steep wavefronts inside the turbulent flow, another objective of this study is to find relations between shock waves in the near-field and events in the turbulent flow. In order to do this, cross-correlations between the flow and sound field are computed to localize the sources of sound, and a conditional-averaging procedure is developed with the aim to describe how steep, asymmetric waves are generated directly from the jet.

The paper is organized as follows. First, the simulation parameters and the numerical methods are presented. The temporal development of the jets are then documented by instantaneous and statistical representations of the flows and the radiated sound fields. Cross-correlations between the turbulent flow inside the jet and the acoustic field are provided in order to localize the dominant sound sources. The presence of shock structures in the radiated pressure field is investigated using high-order statistics and the structure of the acoustic field is studied. Last, a conditional averaging procedure is used to illustrate how steep asymmetric waveforms are generated directly from the shear layers.

## II. Numerical Methodology

### II.A. Initial conditions

Two jets are simulated at diameter based Reynolds numbers  $Re_D = u_j D / \nu$  of 3125 and 12500, where  $u_j$  is the jet initial centerline axial velocity,  $D = 2r_0$  is the jet initial diameter and  $\nu$  is the kinematic viscosity. Both jets are isothermal and have a Mach number  $M_j = u_j / a_j = 2$ , where  $a_j$  is the speed of sound inside the jet. The ambient pressure is equal to  $p_\infty = 10^5$  Pa and the ambient temperature is set to  $T_\infty = 293$  K. At initial time, an axisymmetric hyperbolic-tangent velocity profile is used to initialize the simulations with a realistic laminar flow, and the corresponding density profile is computed using the Crocco-Busemann relation. The initial profiles of density and axial velocity are shown in figure 1 for the two simulated cases, and simulation parameters are shown in table 1. The momentum thicknesses of the shear layers are set to  $\delta_\theta = 2r_0 / \sqrt{Re_D}$ , following the variations of  $\delta_\theta / r_0$  with Reynolds number for initially laminar subsonic jets provided by Zaman.<sup>33</sup> In order to drive the transition of the initial flow from laminar to turbulent state, small velocity perturbations are added in the shear layers. They consist of solenoidal Gaussian vortex rings of random amplitude and phase, as proposed in Bogey<sup>30</sup> for a temporally-developing subsonic round jet. These vortices are regularly distributed in the axial direction with a spacing equal to  $\Delta z = 0.025r_0$  and their maximum velocity randomly fixed between 0 and  $0.04u_j$ , leading to a peak turbulence intensity of about 1% at  $t = 0$ . For each case, four runs are performed using different random seeds for the shear layers perturbations, and the results are ensemble averaged to enhance the convergence of the spatial statistics.

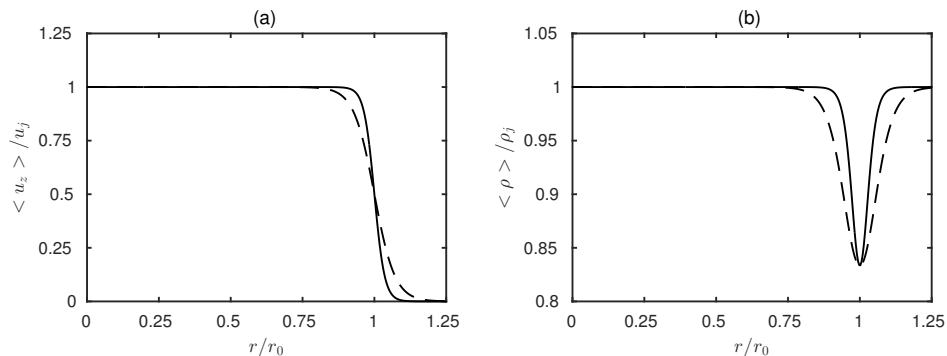


Figure 1. Radial profiles of (a) axial velocity and (b) density at  $t = 0$  for  $Re_D = 3125$  and  $Re_D = 12500$ .

### II.B. Numerical methods

The three-dimensional filtered compressible Navier-Stokes equations are solved in cylindrical coordinates  $(r, \theta, z)$  to compute both the flow and acoustic fields using the low-dissipation and low-dispersion explicit schemes of Bogey & Bailly.<sup>34</sup> In order to remove the singularity on the axis, the method of Mohseni & Colonius<sup>35</sup> is used. The derivatives in the azimuthal direction near the axis are computed using coarser resolutions than permitted by the grid to relieve the restriction on the time-step.<sup>36</sup> More precisely, the effective number of points in the azimuthal direction is progressively varied from 16 for points nearest to the jet axis to 256 for  $r > 0.25r_0$ . Fourth-order eleven-points centered finite difference schemes are used for spatial discretization, and time integration is performed using a second-order six-stage Runge-Kutta algorithm. Grid-to-grid oscillations are removed at every time step by the explicit application of a twelfth-order eleven-point centered filter. At the radial boundary, radiation conditions are prescribed to allow the acoustic waves to exit the computational domain without causing significant spurious reflexions while at the axial boundaries, periodic conditions are enforced to allow the temporal development of the jet.

### II.C. Computational parameters

The mesh grid used for the two simulations extends up to  $z = 240r_0$  in the axial direction, and out to  $r = 13r_0$  in the radial direction. The mesh dimensions in the radial, azimuthal and axial directions are respectively  $n_r = 382$ ,  $n_\theta = 256$  and  $n_z = 9600$  points. In the axial direction, the mesh spacing is uniform and equal to  $\Delta z = 0.025r_0$ . As seen in figure 2, the radial mesh spacing  $\Delta r$  varies in the radial direction. It is minimum

and equal to  $r = 0.006r_0$  at  $r = r_0$  and is maximum and equal to  $0.05r_0$  for  $r \geq 4r_0$ . This yields a Strouhal number of  $St_D = fD/a_\infty = 5$  for an acoustic wave discretized by four points per wavelength. The number of points in the azimuthal direction  $n_\theta = 256$  leads to an equivalent mesh spacing  $r\Delta\theta = 0.024r_0$  at  $r = r_0$ . Last, it has been checked from the computation of turbulent kinetic energy budget that the simulations at  $Re_D = 3125$  and  $Re_D = 12500$  are a fully resolved DNS and a LES, respectively.

The computations are performed using an OpenMP-based in-house solver derived from the one used in Bogey.<sup>30</sup> For the jet at  $Re_D = 12500$ , 8,000 iterations are necessary to reach the final simulation time  $t_f = 72r_0/u_j$ , and 21,000 iterations are necessary to carry out the simulations at  $Re_D = 3125$  until their final simulation time  $t_f = 96r_0/u_j$ . Since the present grid contains about 1 billion points, 200 Gb of memory are used, and a little less than 1,000 CPU hours are necessary to perform 1,000 iterations. As in other temporal numerical simulations,<sup>27</sup> statistical averages are performed over the stationary directions  $\theta$  and  $z$  and the results of the four runs are ensemble averaged. The corresponding mean values are denoted by  $\langle \cdot \rangle$  in what follows, and are thus performed over the equivalent distance of  $4 \times 240r_0 = 960r_0$ .

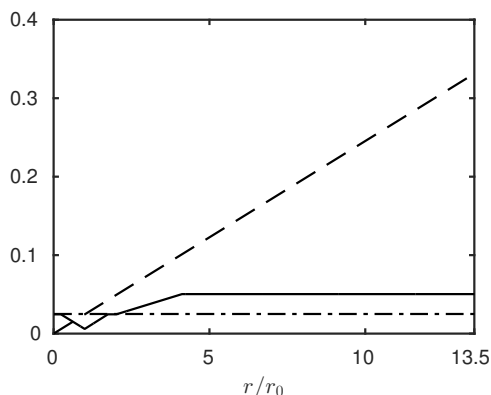


Figure 2. Evolution of the radial, azimuthal and axial mesh spacings —  $\Delta r/r_0$ , - - -  $r\Delta\theta/r_0$  and - · - ·  $\Delta z/r_0$ .

Table 1. Simulation parameters for the two jets.

$Re_D$	$\delta_\theta/r_0$	$t_f u_j/r_0$	$n_{runs}$
3125	$3.6 \cdot 10^{-2}$	96	4
12500	$8.9 \cdot 10^{-3}$	72	4

## III. Results

### III.A. Temporal development of the flow

#### III.A.1. Turbulent flow

Snapshots of the vorticity norm at  $tu_j/r_0 = 25, 50$  and  $72$  are shown in figure 3(a,c,e) for the jet at  $Re_D = 3125$ . In the initial phase of the jet development, the flow consists in an inner potential part surrounded by mixing layers as can be seen in figure 3(a). At this stage, the flow is essentially laminar, although instability waves can be distinguished in the mixing layers. In figure 3(c), at  $tu_j/r_0 = 50$ , the mixing layers from opposite sides of the jet join and merge on the axis. Moreover, large-scale vortices can be observed, and are the result of the temporal growth of the shear-layer instabilities. At  $tu_j/r_0 = 72$ , in figure 3(e), finer turbulent scales can be seen as the flow reaches a fully developed turbulent state. Snapshots of the vorticity norm for the jet at  $Re_D = 12500$  at  $tu_j/r_0 = 12, 25$  and  $50$  also shown in figure 3(b,d,f). The flow representations show that the jet at  $Re_D = 12500$  grows in time in the same fashion as the lower Reynolds number jet. However, a wider range of turbulent scales are distinctly seen at all simulation times, which is a well known effect of increasing Reynolds number in turbulent sheared flows.

Time evolutions of the mean centerline axial velocity and of the shear layer momentum thickness are represented in figure 4 for the two Reynolds numbers considered. In the initial phase of the jet development, the axial velocity remains constant and equal to the jet initial centerline velocity. This is consistent with the

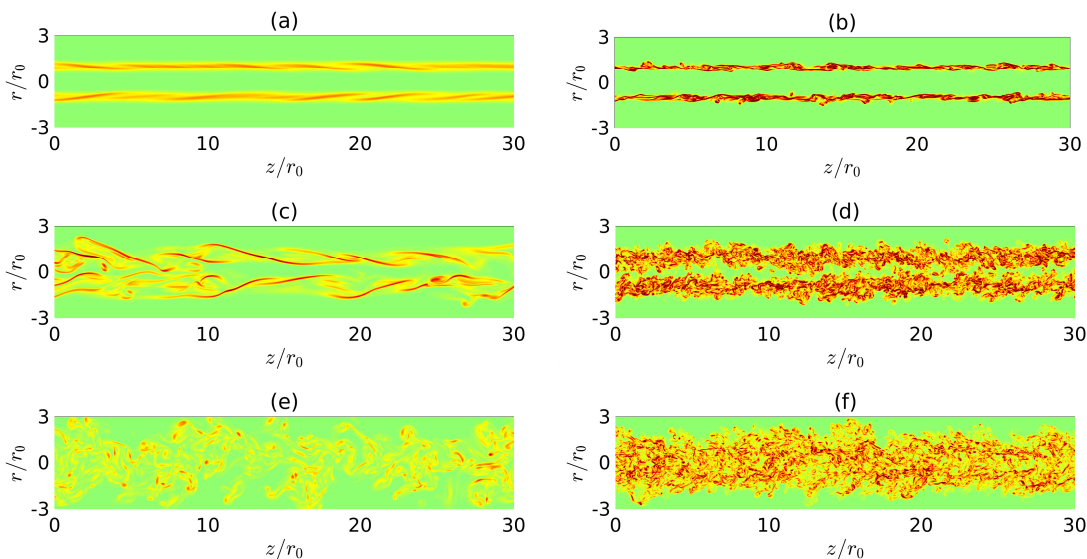


**Figure 3.** Snapshots of vorticity norm for the jet at  $Re_D = 3125$  at (a)  $tu_j/r_0 = 25$ , (c)  $tu_j/r_0 = 50$ , (e)  $tu_j/r_0 = 72$ , and for the jet at  $Re_D = 12500$  at (b)  $tu_j/r_0 = 12$ , (d)  $tu_j/r_0 = 25$  and (f)  $tu_j/r_0 = 37$ . The color scale ranges up to  $5u_j/r_0$ .

snapshots shown in figure 3(a,b), where the inner part of the flow appears to be free from turbulent motion. The mean centerline velocity then begins to decay rapidly as a result of the intrusion of turbulent flow on the jet axis. The axial velocity of the jet at  $Re_D = 12500$  reaches 95% of its initial value at  $tu_j/r_0 = 24$ , which defines the time of the potential core closure  $t_c$ . For the jet at  $Re_D = 3125$ , the closure of the potential core occurs later, at  $tu_j/r_0 = 49$ . In figure 4(b), the shear-layer growth rate is low between  $t = 0$  and  $tu_j/r_0 = 10$  for the jet at  $Re_D = 12500$ , as long as the shear layers are in a laminar state. As the jet transitions from laminar to turbulent state, the spreading rate increases and stay high until the jet reaches a fully developed turbulent state at around  $tu_j/r_0 = 35$ . For the jet at  $Re_D = 3125$ , the initial laminar phase lasts until  $tu_j/r_0 = 40$ , which is a consequence of the damping effect of viscosity on the instability waves of mixing layers, as documented by Morris<sup>37</sup> in the case of incompressible spatially developing round jets. The longer duration of the initial laminar phase of the mixing layer development for the jet at  $Re_D = 3125$  explains why the potential core closure occurs later in this case than for the jet at  $Re_D = 12500$ .

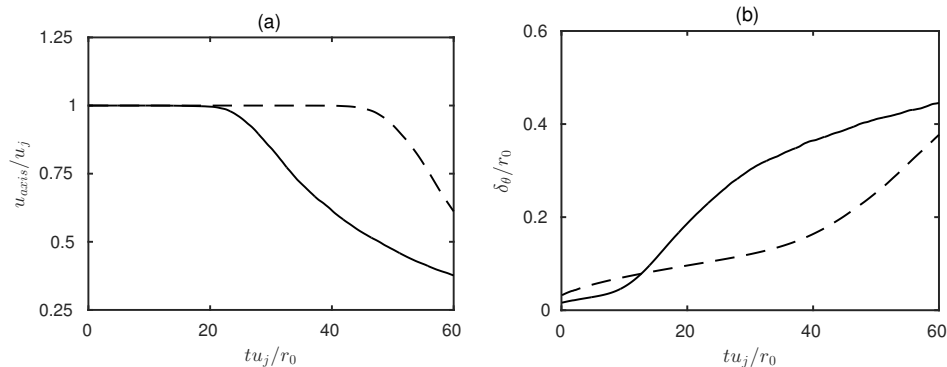


**Figure 4.** Time evolution of (a) mean centerline axial velocity  $u_{axis}$  and (b) momentum thickness  $\delta_\theta$  for the jets at  $Re_D = 12500$  and  $Re_D = 3125$ .

The time evolution of the root-mean-square values of the axial velocity fluctuations is shown in figure 5. For the jet at  $Re_D = 3125$ , a peak value of  $0.20u_j$  is reached nearly simultaneously on the jet axis and in the shear layers at around  $tu_j/r_0 = 50$ , at the closure of the potential core. For the jet at  $Re_D = 12500$ , the peak of axial velocity fluctuations occurs at  $tu_j/r_0 = 14$  at  $r = r_0$ , well before the potential core closure at  $t_c = 24r_0/u_j$ , and is equal to  $0.21u_j$ . On the jet axis, the peak of turbulence intensity is found later, at  $tu_j/r_0 = 31$  where its value reaches  $0.1u_j$ . Significant turbulence intensities are thus found in the mixing layers of the jet at  $Re_D = 12500$ , whereas they remain low until the closure of the potential core for the jet

at  $Re_D = 3125$ .

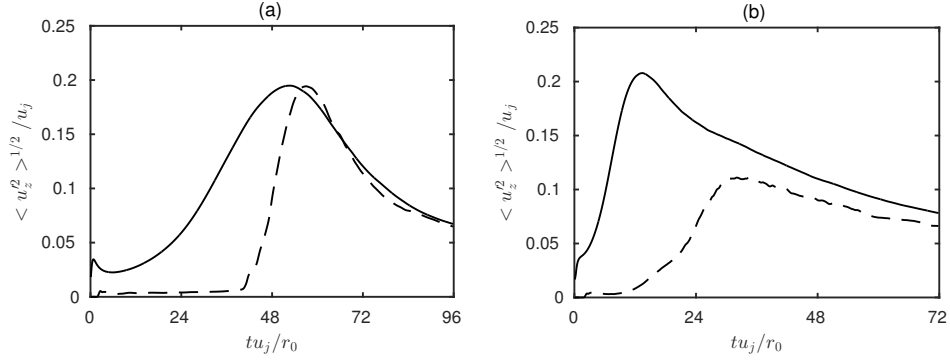


Figure 5. Evolution of the RMS value of the axial velocity fluctuations  $\langle u'^2 \rangle^{1/2} / u_j$  for the jets at (a)  $Re_D = 3125$  and (b)  $Re_D = 12500$  at  $\text{---} r = r_0$  and  $\text{- - -} r = 0$ .

### III.A.2. Sound field

Snapshots of vorticity norm and pressure fluctuations are presented in figure 6(a,b) at  $tu_j/r_0 = 50$  and  $72$  for the jet at  $Re_D = 3125$ . At  $tu_j/r_0 = 50$ , the potential core closes. In the acoustic field, highly directional pressure waves emerge from the flow, and are attached to turbulent structures inside the jet. At  $tu_j/r_0 = 72$ , stronger waves are seen to be radiated from the turbulent flow, and are also very directive. Moreover, the sound field appears to be less regular, and covers a wider range of wavenumbers. Similarly, instantaneous representations of the jet at  $Re_D = 12500$  at  $tu_j/r_0 = 25$  and  $50$  are given in figure 6(c,d). At  $tu_j/r_0 = 25$ , the pressure field is once again dominated by strong, directive waves emanating from the shear layers. In comparison with the sound field produced by the jet at  $Re_D = 3125$ , the frequency of occurrence of these waves is strongly increased. At  $tu_j/r_0 = 50$ , fewer waves are visible, the pressure levels are reduced and the sound field seems to be dominated by a lower frequency component. For the present jet conditions, the expected Mach wave radiation angle  $\alpha$  can be evaluated using (1), where the convection velocity  $u_c$  is estimated using

$$\frac{u_c}{a_\infty} = \frac{1 + M_j}{1 + a_\infty/a_j}, \quad (2)$$

following Oertel.<sup>38</sup> For the present initial conditions, expression (2) yields  $u_c = 0.75u_j$ , hence  $\alpha = 48.2^\circ$ . The expected Mach wave orientation is represented by a solid line in figure 6 and is in good agreement with the global directivity of the sound field visible in figure 6(b,c,d). It however appears to overestimate the angle of directivity in figure 6(a).

The time evolution of the standard deviation of the pressure fluctuations is shown in figure 7(a,b) as a function of time and radial coordinate. For the two cases considered, a lobe of sound emission is seen to emerge from the jet. This lobe is generated between  $tu_j/r_0 = 48$  and  $tu_j/r_0 = 72$  for the jet at  $Re_D = 3125$ , which is just after the closure of the potential core. For the jet at  $Re_D = 12500$ , the peak of sound emission originates between  $tu_j/r_0 = 12$  and  $tu_j/r_0 = 45$ , which means that sound emission is significant before and after the closure of the potential core at  $tu_j/r_0 = 25$ . At  $r = 8r_0$ , the peak of sound intensity occurs at  $tu_j/r_0 = 35$  for the jet at  $Re_D = 12500$  and at  $tu_j/r_0 = 70$  for the jet at  $Re_D = 3125$ . The maximum sound pressure levels at this radial location are 1300 Pa and 1500 Pa for the jets at  $Re_D = 3125$  and  $Re_D = 12500$ , respectively.

### III.B. Space-time cross-correlations between the flow and the sound field

Space-time cross-correlations between the acoustic field and flow variables inside the jet are an useful tool to find relations between a given flow and its radiated sound field. They have been used in many experimental and numerical investigations of sound generation in spatially-developing jets.<sup>16,39-41</sup> More recently, they have also been computed for a temporal subsonic round jet.<sup>30</sup> The pressure fluctuations at position  $(r = r_2, \theta, z)$  and time  $t_2$  are correlated with the axial velocity fluctuations  $u'_z$  at position  $(r = r_1, \theta, z + \delta z)$  at time  $t_1$ .

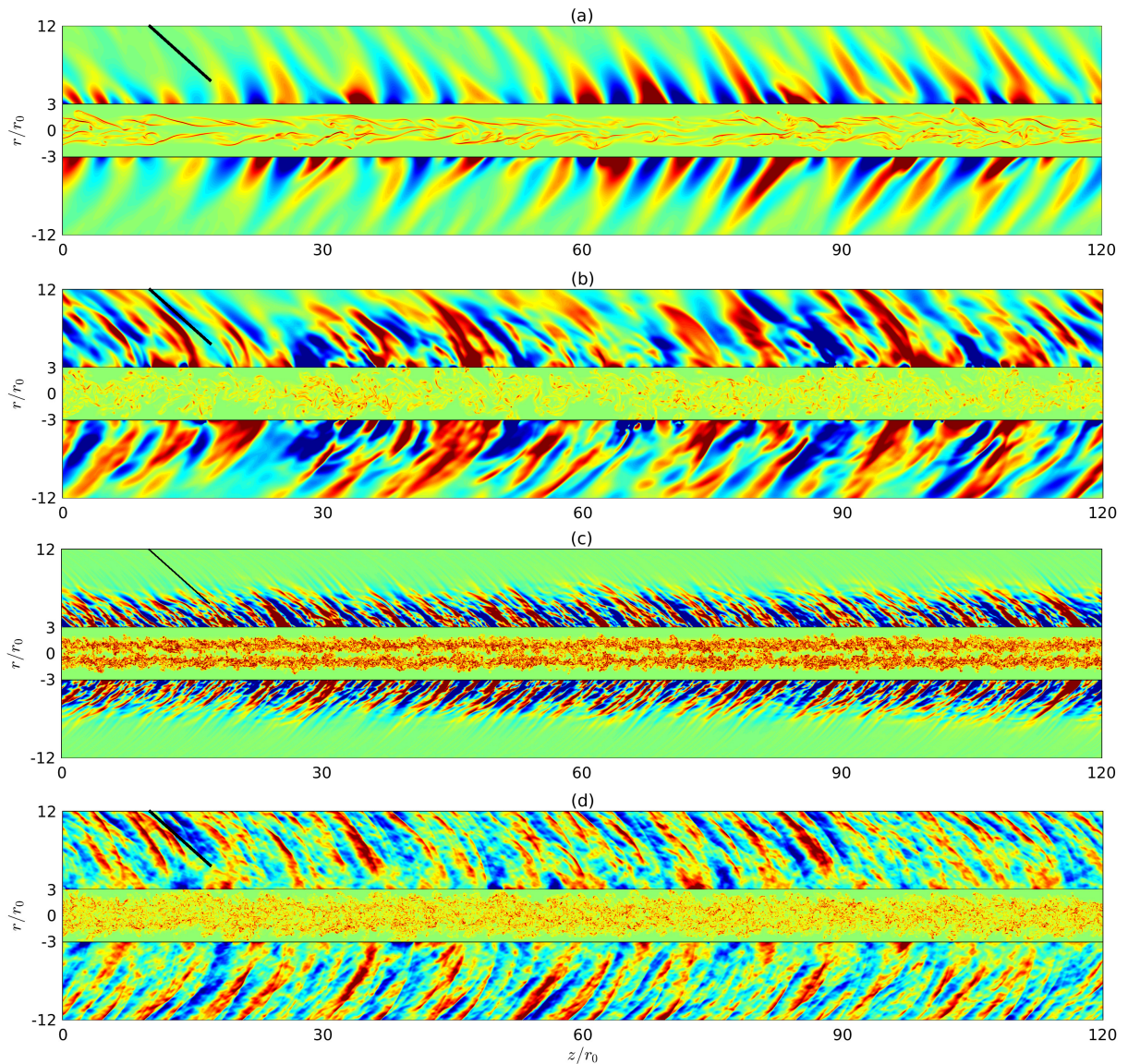


**Figure 6.** Snapshots of vorticity norm and of pressure fluctuations for the jet at  $Re_D = 3125$  at (a)  $tu_j/r_0 = 50$ , (b)  $tu_j/r_0 = 72$  and for the jet at  $Re_D = 12500$  at (c)  $tu_j/r_0 = 25$  and (d)  $tu_j/r_0 = 50$ . The color scale ranges up to  $5u_j/r_0$  for the vorticity norm and from  $-2500$  to  $2500$  Pa for the pressure fluctuations. The solid line indicates the expected orientation of the Mach waves computed using equation (2).

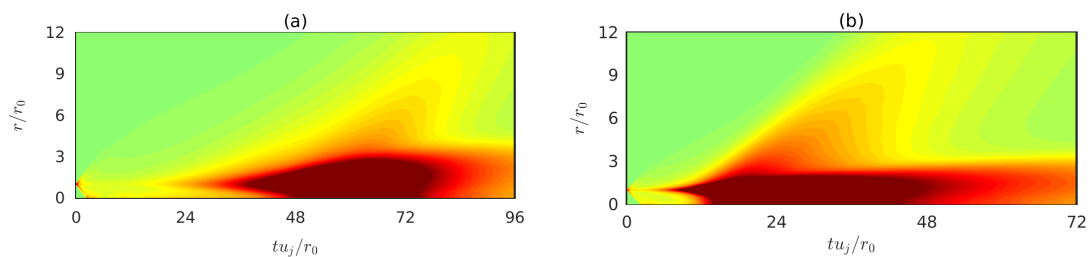


**Figure 7.** Representation of the standard deviation of the pressure fluctuations  $\langle p'^2 \rangle^{1/2}$  for the jets at (a)  $Re_D = 3125$  and (b)  $Re_D = 12500$ . The color scale ranges up to  $5000$  Pa.

The correlation function is thus given by :

$$C_{u'_z p'}(\delta z, t_1) = \frac{\langle u'_z(r_1, \theta, z + \delta z, t_1) p'(r_2, \theta, z, t_2) \rangle}{\langle u'_z(r_1, \theta, z, t_1)^2 \rangle^{1/2} \langle p'(r_2, \theta, z, t_2)^2 \rangle^{1/2}}. \quad (3)$$

In this study, the correlations between the pressure fluctuations at  $r = 8r_0$  and the axial velocity fluctuations at  $r = 0.4r_0$  are shown in figure 8(a) for the jet at  $Re_D = 12500$ . The time of the potential core closure is indicated by a dashed line and the solid line denotes propagation at the ambient speed of sound between the source and the observer points. Since the solid line lies below the dashed line, the sound field at  $r = 8r_0$  and  $t_2 = 35r_0/u_j$  is generated before the closure of the potential core. Significant negative levels of correlation are found in a narrow and elongated region extending over  $15r_0$  in the axial direction, and over 10 time units. This suggests that the portion of fluid correlated with the sound field is moving in the downstream direction while remaining coherent in time and space. Moreover, the orientation of the correlation spot provides a convection velocity close to  $0.75u_j$ , which is higher than the ambient speed of sound. This strongly supports that a significant part of the sound waves radiated by the temporal jet before the closure of the potential core are Mach waves. Likewise, the correlation function between the pressure field at  $r = 8r_0$  and  $t_2 = 50r_0/u_j$  and axial velocity fluctuation on the jet axis is represented in figure 8(b) for the jet at  $Re_D = 12500$ . The solid line corresponding to propagation at the ambient speed of sound crosses the dashed line at  $t_1 = 25$  for  $\delta z = -10r_0$ . This means that the waves obtained at  $r = 8r_0$  and  $t_2 = 50r_0/u_j$  can be generated during or after the closure of the potential core. Once again, the orientation of the correlation spot is consistent with the motion of the sound sources at a speed close to  $0.75u_j$ .

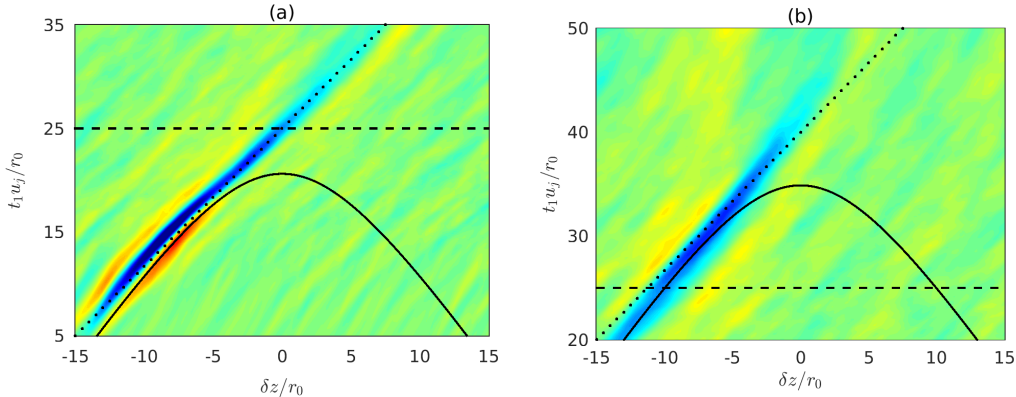


**Figure 8.** Representation of the normalized space-time cross-correlations for the jet at  $Re_D = 12500$  (a) between pressure fluctuations at  $r = 8r_0$  and  $t = t_2 = 35r_0/u_j$  and axial velocity fluctuations at  $r = 0.4r_0$  and  $t = t_1$  and (b) between pressure fluctuations at  $r = 8r_0$  and  $t = t_2 = 50r_0/u_j$  and axial velocity fluctuations at  $r = 0$  and  $t = t_1$ . The solid line indicates propagation at the ambient speed of sound, the dashed line marks the time  $t_c$  of the potential core closure and the dotted line represents a convection at a speed of  $0.75u_j$  inside the jet. The color scale ranges from  $-0.25$  to  $0.25$ .

The radial profiles of the maximum absolute value of the normalized correlations between the pressure fluctuations at  $r = 8r_0$  and the velocity fluctuations inside the jet are displayed in figure 9. For the sound field at  $t_2 u_j / r_0 = 35$ , a peak correlation of 0.3 is reached at around  $r = 0.4r_0$  for the axial component of the velocity fluctuations. The dotted line in figure 9 indicates the radial position where the mean vorticity norm reaches 1% of its maximum value at  $t = t_1 = 12r_0/u_j$ , when the correlation with the axial velocity at  $r = 0.4r_0$  is maximum. It suggests that the turbulent structures at the origin of Mach waves are located in the inner part of the shear layers. This observation is consistent with the results of Papamoschou & Bunyajitradulya<sup>42</sup> who found evidence of coherent structures traveling at speeds very close to the freestream velocity in spatially developing supersonic-subsonic mixing layers. It is also in agreement with the vortex-train model proposed by Oertel<sup>38</sup> to describe Mach wave radiation. Moreover, the value of the peak correlations between the sound field at  $t_2 u_j / r_0 = 50$  and the velocity fluctuations seems to be independent of the radial location at which it is computed, as shown in figure 9(b). The sound sources at this simulation time thus appear to be homogeneously distributed inside the jet.

### III.C. Shock structures in the radiated pressure field

The presence of steep, asymmetric pressure waveforms near high-speed supersonic jets has been revealed by acoustic measurements, and have been associated with the perception of crackle noise.<sup>12</sup> One popular metric

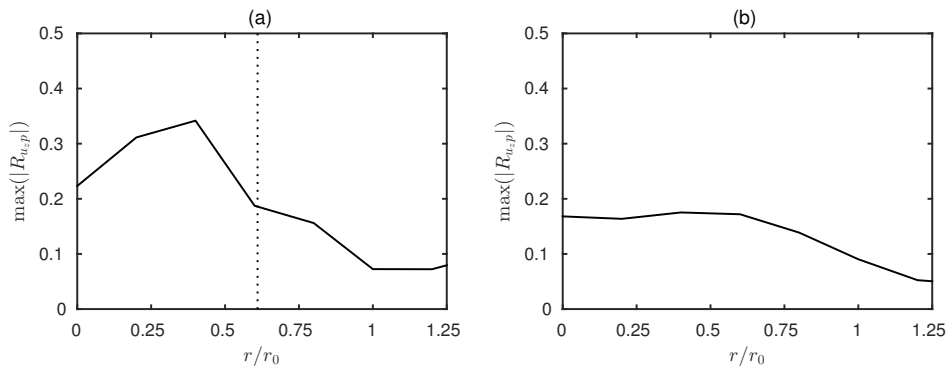


**Figure 9.** Representation of the radial evolution of the maximum modulus of the normalized space-time cross-correlation function between (a) pressure fluctuations at  $(r = 8r_0, t = 35r_0/u_j)$  and axial velocity fluctuations  $u'_z$  at  $(r, t_1)$ , and (b) pressure fluctuations at  $(r = 8r_0, t = 50r_0/u_j)$  and axial velocity fluctuations  $u'_z$  at  $(r, t_1)$ . The dotted line in (a) indicates the position where  $\langle |\omega| \rangle = 0.01 \langle |\omega_{max}| \rangle$  at  $t = 12r_0/u_j$ .

used to quantify the asymmetry of a waveform is the skewness factor of the pressure fluctuations, defined as

$$S(p') = \frac{\langle p'^3 \rangle}{\langle p'^2 \rangle^{3/2}}. \quad (4)$$

In the past, crackle noise has been correlated with values of  $S(p')$  higher than 0.4.<sup>12</sup> However, as pointed out by Gee,<sup>43</sup> high levels of skewness of the pressure fluctuations do not necessarily lead to the perception of crackle noise. Rather, this peculiar sound is often attributed to the presence of fast compressions followed by gradual expansions. This latter feature can be quantified by computing the skewness factor of the time derivative of the pressure fluctuations.<sup>15</sup> The skewness factors of the pressure fluctuations and of their time derivative for the two present jets are represented in figure 10 as a function of time and radial coordinate. Contours of sound pressure levels are also shown for comparison. For both jets, positive values of  $S(p')$  are seen in figure 10(a,b), suggesting the presence of intermittent positive bursts in the pressure field. The regions where  $S(p')$  is high are located in the immediate vicinity of the flow and originate from  $tu_j/r_0 = 40$  to  $tu_j/r_0 = 70$  for the jet at  $Re_D = 3125$ , and from  $tu_j/r_0 = 10$  to  $tu_j/r_0 = 35$  for the jet at  $Re_D = 12500$ . The maximum values of  $S(p')$  are 0.8 and 0.7, respectively. In addition, positive values of skewness of the pressure time derivative are found for both jets, as in figure 10(c,d). They are located in the immediate vicinity of the flow, which supports the idea that crackle noise is mainly the result of a source mechanism. Interestingly, the contours of  $S(dp/dt)$  are oriented in the same way as the contours of pressure fluctuations. This is in contrast with what is observed for the contours of  $S(p')$ , for which no clear link can be established with sound intensity.

The axial evolution of the pressure fluctuations at  $r = 8r_0$  for the jet at  $Re_D = 3125$  is shown in figure 11 at  $tu_j/r_0 = 70$  and  $tu_j/r_0 = 90$ . At  $tu_j/r_0 = 70$ , the pressure fluctuations signal intermittently shows high positive values as, for example, at  $z = 180r_0$  and  $z = 220r_0$ , where it exceeds three times its standard deviation. Moreover, the waveform at this simulation time exhibits fast compressions followed by more gradual expansions, and is thus similar to those found in previous studies of crackle noise.<sup>7,44</sup> At  $tu_j/r_0 = 90$ , no significant asymmetry is found in the pressure signal. However, steep compressions appear as, for example, at  $z/r_0 = 5$  and  $z/r_0 = 215$ , although they are less frequent than at  $tu_j/r_0 = 70$ .

### III.D. Structure of the radiated pressure field

#### III.D.1. Two-dimensional spatial correlations of the pressure fluctuations

The two-dimensional spatial correlation function of the pressure fluctuations  $R_{zr}(\delta z, \delta r)$  at  $r = 8r_0$  is computed using the relation

$$R_{zr}(\delta z, \delta r) = \frac{\langle p'(r + \delta r, \theta, z + \delta z, t)p'(r, \theta, z, t) \rangle}{\langle p'(r, \theta, z, t)^2 \rangle}, \quad (5)$$

and is shown in figure 12 at  $tu_j/r_0 = 35, 45$  and  $55$  for the jet at  $Re_D = 12500$ . At  $tu_j/r_0 = 35$ , as the sound intensity reaches its peak value, significant levels of correlation are found in a narrow and straight region,

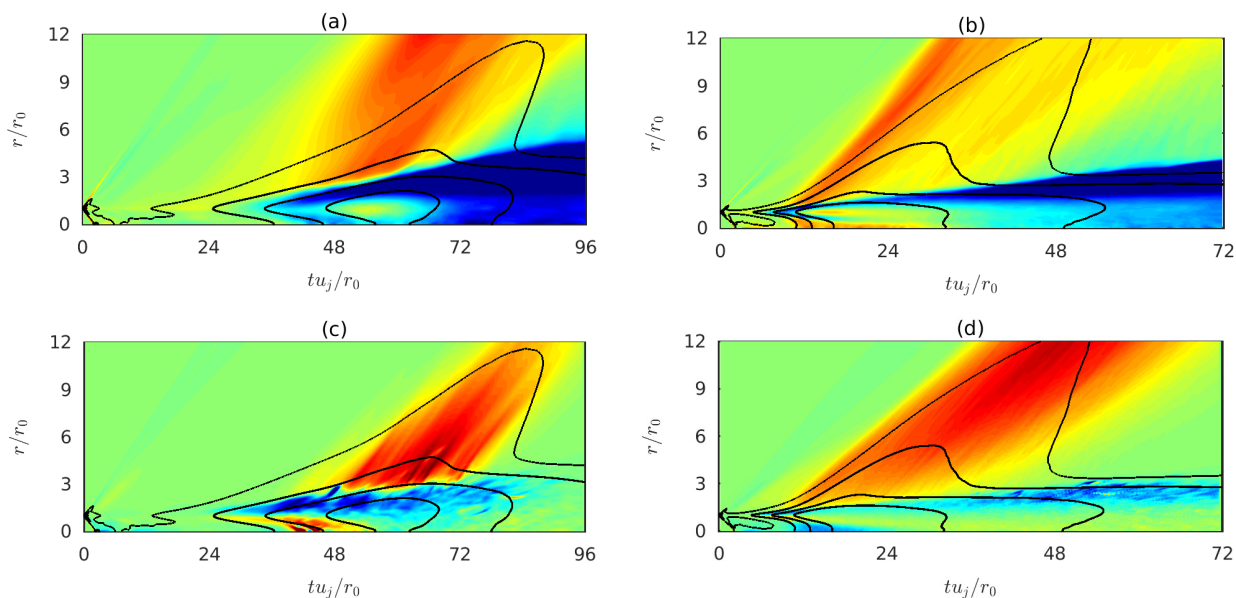


Figure 10. Representation of (a,b) the skewness factor of the pressure fluctuations and (c,d) the skewness factor of the pressure time derivative for the jet at (a,c)  $Re_D = 3125$  and (b,d)  $Re_D = 12500$ . The color scales range (a,b) from -1 to 1 and (c,d) from -2 to 2. The solid lines indicate the contours of the RMS value of the pressure fluctuations  $\langle p'^2 \rangle^{1/2}$  at 1000 Pa, 2000 Pa, 4000 Pa and 8000 Pa.

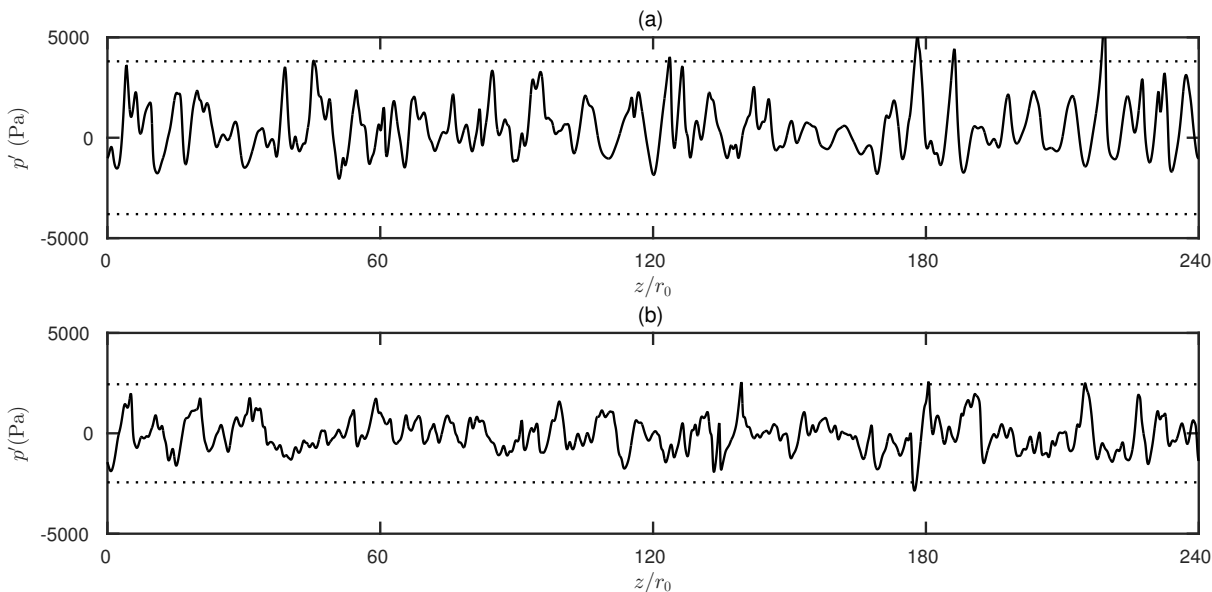
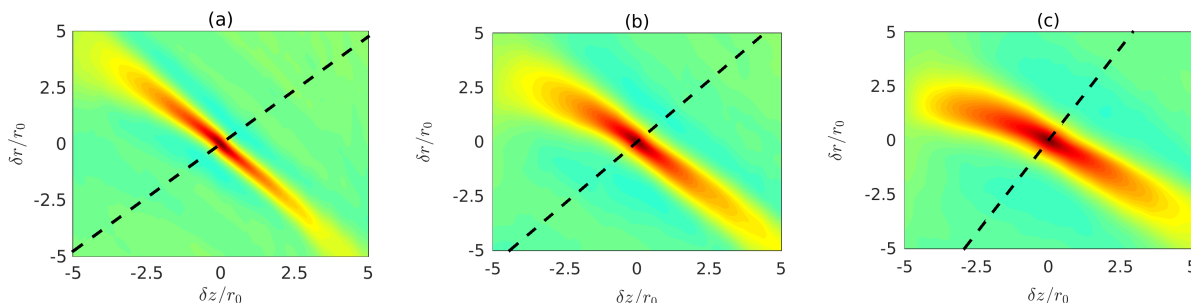


Figure 11. Axial evolution of the pressure fluctuations at  $r = 8r_0$ ,  $\theta = 0$  at (a)  $tu_j/r_0 = 70$  and (b)  $tu_j/r_0 = 90$  for the jet at  $Re_D = 3125$ . The dotted lines indicate the value of  $\pm 3 \langle p'^2 \rangle^{1/2}$ .

which supports the important directivity of the sound field. At  $tu_j/r_0 = 45$  and  $tu_j/r_0 = 55$ , the correlation spot is wider although its shape remains narrow and elongated. In addition, the orientation of the correlation spot becomes more and more inclined with time, indicating an increase of the global radiation angle. In the snapshots of pressure fluctuations shown in figure 6(d), the acoustic field at  $tu_j/r_0 = 50$  consists in straight, narrow wavefronts corresponding to Mach waves that are superimposed on lower-frequency components. The emergence of these lower-frequency components, as well as the relative decrease of the contribution of Mach wave radiation to the global sound field may explain the qualitative evolution of the correlation function of the pressure fluctuations.



**Figure 12.** Representation of the 2-D spatial correlations of pressure fluctuations at  $r = 8r_0$  for the jet at  $Re_D = 12500$  at (a)  $tu_j/r_0 = 35$ , (b)  $tu_j/r_0 = 45$ , and (c)  $tu_j/r_0 = 55$ . The dashed line indicates the mean direction of propagation, and the color scale ranges from -1 to 1.

### III.D.2. Local wave directivity

In order to isolate the contribution of steep compression waves to the global directivity of the sound field, a measure of the local orientation of the wavefronts is defined at position  $(r, \theta, z)$  as the angle  $\alpha_l$  corresponding to the direction of the pressure gradient. It is computed using the relation

$$\alpha_l(r, \theta, z, t) = \tan^{-1} \left( \frac{\frac{dp}{dr}(r, \theta, z, t)}{\frac{dp}{dz}(r, \theta, z, t)} \right), \quad (6)$$

only in the regions where the dilatation  $\Theta = \nabla \cdot \mathbf{u}$  is lower than a negative threshold  $\sigma_\Theta$ , so as to put emphasis on regions of high compressibility. This is illustrated in figure 13 where a contour of dilatation corresponding to the threshold  $\sigma_\Theta = -3 < \Theta'^2 >^{1/2}$  is shown over a representation of the pressure fluctuations. The radiation angles are thus only computed in the regions located inside this contour. In addition, a condition based on the local pressure difference is added in order to retain only waves of significant energy. More precisely, for each point satisfying the condition on dilatation, the maximum and the minimum of the pressure fluctuations are computed in the direction specified by the pressure gradient and only points where the pressure jump  $\Delta p$  is higher than a threshold  $\sigma_p$  are selected for the conditional averaging. This procedure is performed over the four cuts of the pressure field at  $\theta = 0, 90^\circ, 180^\circ$  and  $270^\circ$  for the four different runs. The computations have been carried out using different values of the threshold parameters, and it was found that for  $\sigma_\Theta = -3 < \Theta'^2 >^{1/2}$  and  $\sigma_p = 2 < p'^2 >^{1/2}$ , all detected shock events satisfied the Rankine-Hugoniot jump condition. Moreover, the results obtained using different values of  $\sigma_\Theta$  and  $\sigma_p$  are qualitatively similar, and the present values are thus used for all the results presented in this paper. The time evolution of the number of shock events detected by the present algorithm at  $r = 8r_0$  is represented in figure 14(a,b) for the two jets. The peak of shock detection appears to be located at  $tu_j/r_0 = 70$  and at  $tu_j/r_0 = 35$  for the jets at  $Re_D = 3125$  and  $Re_D = 12500$ , respectively. In both cases, it corresponds to the time of maximum sound emission. For the jet at  $Re_D = 3125$ , a number of 750 shock events are detected over the four runs at  $tu_j/r_0 = 70$ , while 1500 events are found for  $Re_D = 12500$  at  $tu_j/r_0 = 35$ . After this peak, the number of detections gradually decreases and is lower than 100 for  $tu_j/r_0 \geq 55$  for  $Re_D = 12500$ . The time evolution of the mean pressure jump for the two jets is displayed in figure 15(a,b). It also peaks at the time of maximum sound emission for the two Reynolds numbers considered. The mean pressure variation across the shocks at the peak of sound emission is equal to 3500 Pa for  $Re_D = 3125$  and to 5000 Pa for  $Re_D = 12500$ . The Reynolds number thus appears to have a significant effect on the frequency of occurrence of the shock waves, as well as on their strength.

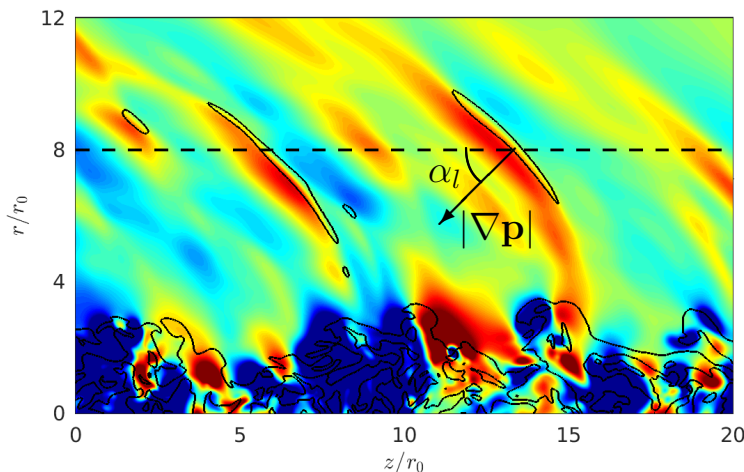


Figure 13. Representation of the pressure fluctuations at  $tu_j/r_0 = 70$  for the jet at  $Re_D = 3125$ . The solid line indicates the contour of  $\Theta = \sigma_\Theta$ , where  $\sigma_\Theta = -3 < \Theta^2 >^{1/2}$  is the dilatation threshold. The dashed line indicates the radial location where the conditional averaging is performed and the color scale ranges from -5000 Pa to 5000 Pa.

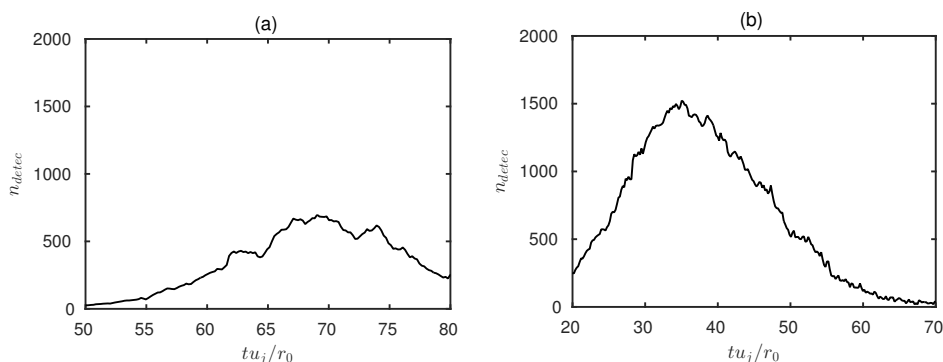


Figure 14. Time evolution of the number of detected shock events at  $r = 8r_0$  for the four runs for the jets at (a)  $Re_D = 3125$  and (b)  $Re_D = 12500$ .

For all detected shock events, the local radiation angle is computed at  $r = 8r_0$  using relation (6), and the results are averaged to obtain a mean shock-front radiation angle. The evolution of this angle is shown in figure 16. The global directivity angle computed from the orientation of the two-dimensional correlations and the Mach wave angle  $\alpha_{th} = 48.2^\circ$  computed using Oertel's empirical relation are also displayed. For the two jets considered, the mean shock front angle remains practically constant at all simulation times, whereas the global radiation angle continuously decreases. The directivity of the shock fronts is thus different from that of the global sound field. For the jet at  $Re_D = 3125$ , the difference between the two angles is minimum at  $tu_j/r_0 = 60$  where it is equal to  $15^\circ$ , and reaches a maximum of  $25^\circ$  at  $tu_j/r_0 = 80$ . For the jet at  $Re_D = 12500$ , the value of the mean shock front angle lies within  $5^\circ$  of the global radiation angle from  $tu_j/r_0 = 30$  to  $tu_j/r_0 = 45$ . Afterward, the difference between the two increases to reach  $15^\circ$  at  $tu_j/r_0 = 55$ . The present results thus suggest that the directivity of the steep, strong waves radiated by the two temporal jets remains almost unchanged during the temporal development of the jet, whereas the global directivity of the sound field evolves toward shallower directions from the jet axis.

The orientation of a Mach wave emerging from the jet is linked to the convection velocity of its source by the relation (1). The local radiation angles  $\alpha_l$  of the shock events detected by the present algorithm are thus used to estimate the statistical distribution of the convective velocities of the sources of these waves. The probability density function of the shock front radiation angles at  $r = 8r_0$  is shown in figure 17 at  $tu_j/r_0 = 70$  for the jet at  $Re_D = 3125$  and at  $tu_j/r_0 = 35$  for the jet at  $Re_D = 12500$ . The histograms are centered around  $0.75u_j$ , which is the convection velocity predicted using expression (2). Interestingly, they have large positive tails. It suggests that waves generated by the motion of turbulent structures at

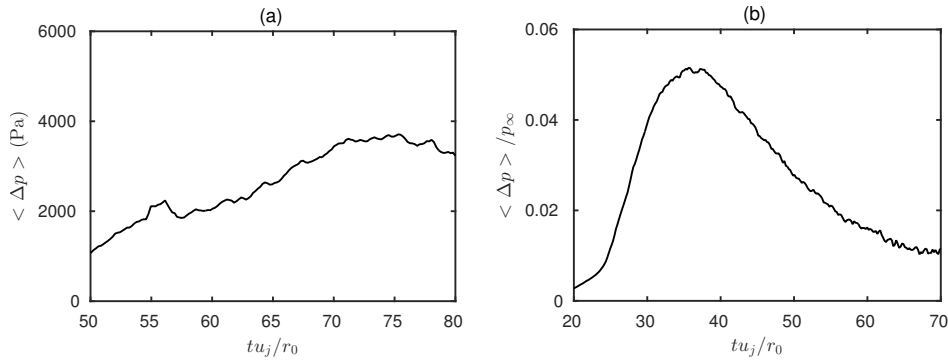


Figure 15. Time evolution of the mean pressure jump across the shocks detected at  $r = 8r_0$  for the jet at (a)  $Re_D = 3125$  and (b)  $Re_D = 12500$ .

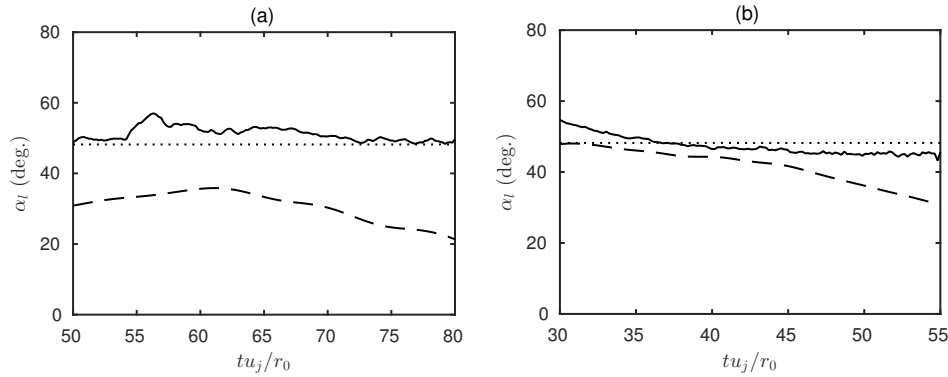


Figure 16. Time evolution of the radiation angle for the jets at (a)  $Re_D = 3125$  and (b)  $Re_D = 12500$  computed at  $r = 8r_0$  using — conditional averaging, - - - 2D spatial correlations and ..... relation (2).

speeds significantly higher than the mean convection velocity are found at these simulation times. The same observations have recently been made by Murray & Lyons<sup>24</sup> who measured the orientation of weak shock waves in the near field of supersonic jets using optical measurements.

### III.E. Conditional averaging of shock wave generation

In figure 6(c) several shock structures are found to be generated in the mixing layers of the temporal jet at a given simulation time. Since the present flow is stationary in the axial direction, a conditional averaging procedure can be used to extract the generic characters of these shock structures and of their generation process. The axial profile of the dilatation  $\nabla \cdot \mathbf{u}$  at  $r = 2.5r_0$  is displayed in figure 18 for the jet at  $Re_D = 12500$ . Strong intermittent negative spikes can be distinctly seen and indicate the locations of shock waves in the near field of the jet. The dilatation at  $r = 2.5r_0$  is thus used as a trigger signal in a conditional averaging procedure : when its value falls below a negative threshold, the flow field is recorded over a window centered around the position  $z_{trig}$  of the local minimum of dilatation and extending over  $10r_0$  in the axial direction and from  $r = 0$  to  $r = 5r_0$  in the radial direction. The corresponding flow representations are then synchronized with the minimum of dilatation at  $r = 2.5r_0$  and ensemble averaged, such that only generic, coherent features emerge from the background noise. This operation is performed at the detection times  $tu_j/r_0 = 55$  and  $tu_j/r_0 = 16$  for the jets at  $Re_D = 3125$  and  $Re_D = 12500$ , respectively. The conditional averaging is carried out over the cuts of the flow at  $\theta = 0^\circ, 90^\circ, 180^\circ$  and  $270^\circ$  for all four simulated runs. In order to extract information on the shock waves generation process, the flows at previous and subsequent times are also ensemble averaged using the windows computed at the detection times.

Snapshots of the conditionally-averaged pressure fluctuations for the jet at  $Re_D = 3125$  are represented in figure 19 at  $tu_j/r_0 = 51, 55$  and  $59$ , with contours of conditionally averaged vorticity. At  $tu_j/r_0 = 51$ , a positive pressure wave is seen to emerge from the flow at  $(z - z_{trig})/r_0 = -2.5$ . Meanwhile, significant levels

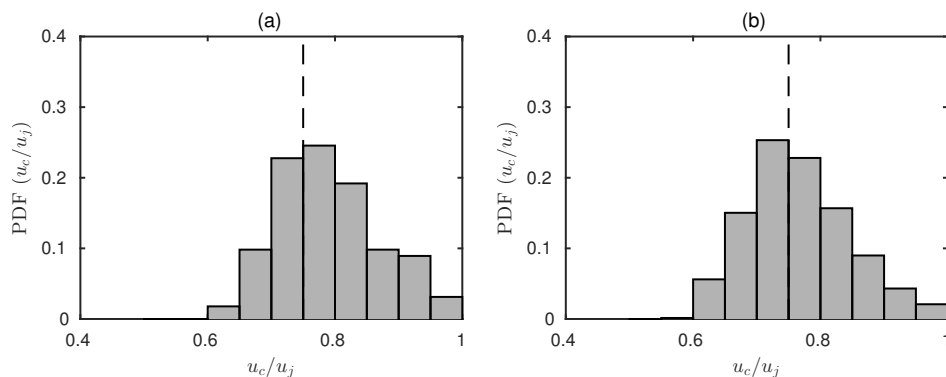


Figure 17. Representation of the probability density function of the convection velocities of source events at the origin of the shock waves detected at  $r = 8r_0$  (a) for the jet at  $Re_D = 3125$  at  $tu_j/r_0 = 70$  and (b) for the jet at  $Re_D = 12500$  at  $tu_j/r_0 = 35$ . The dashed line indicates the convection velocity  $u_c = 0.75u_j$  predicted using (2).

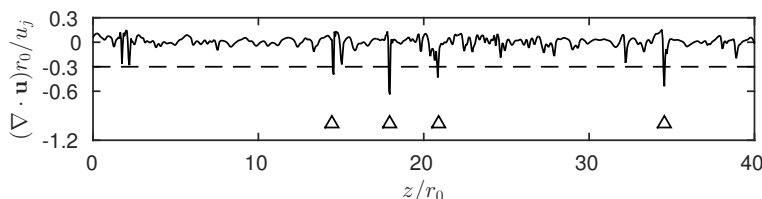


Figure 18. Axial evolution of the dilatation at  $r = 2.5r_0$ ,  $\theta = 0$  and  $tu_j/r_0 = 16$  for the jet at  $Re_D = 12500$ . The dashed line corresponds to the value  $-0.3u_j/r_0$  used as a threshold for shock detection, and the black triangles indicate the positions where shocks are detected.

of vorticity are found on the jet axis, at the lower end of the wavefront. Since the pressure wave is inclined, this is most likely a Mach wave attached to the vorticity spot located on the jet axis. At the detection time  $tu_j/r_0 = 55$ , lower levels of vorticity are found at  $r = 0$  which can be explained by the possible breakdown of the structure at the origin of the pressure wave. This tendency is confirmed at  $tu_j/r_0 = 59$ , where the wave propagates in the downstream direction. Similarly, representations of the conditionally-averaged pressure fluctuations and vorticity for the jet at  $Re_D = 12500$  are represented in figure 20 at  $tu_j/r_0 = 12$ , 16 and 20. In this case, significant levels of vorticity are found in the shear layers at  $tu_j/r_0 = 12$ , suggesting the presence of a coherent structure. Once again, a strong pressure wave is seen to rise from the flow and appears to be connected to the region of high vorticity. At the detection time  $tu_j/r_0 = 16$ , the pressure wave is still attached to the vorticity spot that is located downstream of its former position. The average convection velocity of the turbulent structure can be estimated by measuring its displacement between  $tu_j/r_0 = 12$  and  $tu_j/r_0 = 16$ , yielding  $u_c \simeq 1.6a_\infty$ , which is consistent with Mach wave radiation. At  $tu_j/r_0 = 20$ , no significant levels of vorticity are detected, and the shock wave propagates away from the jet. It thus appears that for the two Reynolds numbers considered, the generation of shock structures in the vicinity of the jet can be attributed to the convection of turbulent structures at supersonic speeds. These turbulent structures are located on the axis for the jet at  $Re_D = 3125$ , but in the shear-layers for the jet at  $Re_D = 12500$ .

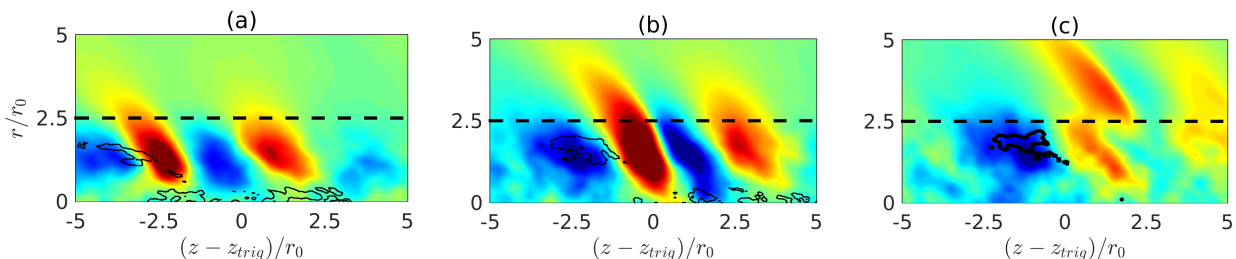
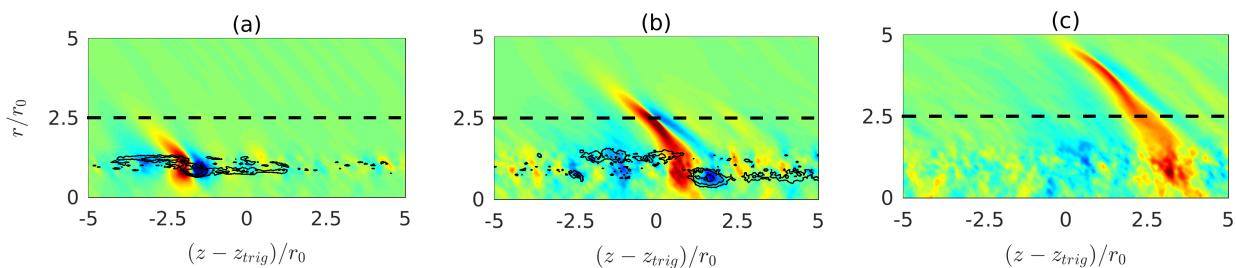
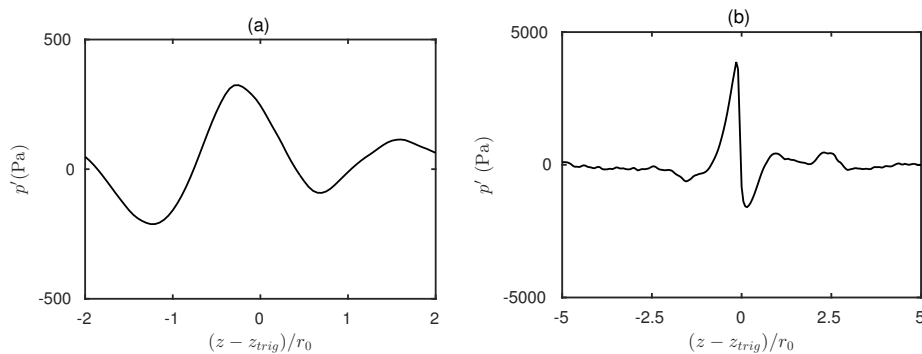


Figure 19. Snapshots of the conditionally averaged pressure fluctuations at (a)  $tu_j/r_0 = 51$ , (b)  $tu_j/r_0 = 55$  and (c)  $tu_j/r_0 = 59$  for the jet at  $Re_D = 3125$ . The solid lines indicate contours of conditionally averaged vorticity corresponding to the values of  $0.18u_j/r_0$ ,  $0.27u_j/r_0$  and  $0.36u_j/r_0$ , and the dashed line marks the radial position  $r = 2.5r_0$  where the shocks are detected. The color scale ranges from -3000 Pa to 3000 Pa.



**Figure 20.** Snapshots of the conditionally averaged pressure fluctuations at (a)  $tu_j/r_0 = 12$ , (b)  $tu_j/r_0 = 16$  and (c)  $tu_j/r_0 = 20$  for the jet at  $Re_D = 12500$ . The solid lines indicate contours of conditionally averaged vorticity corresponding to the values of  $0.2u_j/r_0$ ,  $0.4u_j/r_0$  and  $0.8u_j/r_0$ , and the dashed line marks the radial position  $r = 2.5r_0$  where the shocks are detected. The color scale ranges from -3000 Pa to 3000 Pa.

The evolution of the conditionally averaged pressure fluctuations at  $r = 2.5r_0$  is represented in figure 21 at  $tu_j/r_0 = 12$  and 16 for the jet at  $Re_D = 12500$ . At  $tu_j/r_0 = 12$ , the mean pressure wave has a low amplitude, is symmetric, and both its rise and its decay are gradual. In figure 20, the pressure signal at  $r = 2.5r_0$  corresponds to the upper tail of the averaged pressure wave. It is thus representative of the linear Mach waves generated during the initial instability development of the jet, which explains its rather smooth character. At  $tu_j/r_0 = 16$ , the averaged pressure waveform consists in a weak negative part for  $z > z_{trig}$  followed by a steep compression for  $z < z_{trig}$ , where the pressure fluctuation goes from -1000 Pa to 4000 Pa before gradually decreasing to zero. The conditionally averaged pressure waveform thus has the steep and asymmetric character of the waveforms found in the pressure fields of supersonic jets exhibiting crackle noise. The fact that this waveform is observed in the immediate vicinity of the jet supports the idea that the presence of shock waves in the near field of the jets is mainly the result of a source mechanism.



**Figure 21.** Time evolution of the conditionally averaged pressure fluctuations at  $r = 2.5r_0$  and at (a)  $tu_j/r_0 = 12$  and (b)  $tu_j/r_0 = 16$  for the jet at  $Re_D = 12500$ .

## IV. Conclusion

In this paper, the flow and sound fields of two temporally-developing isothermal supersonic round jets at a Mach number of 2 and at diameter-based Reynolds numbers of 3125 and 12500 are presented. They are computed on grids extending up to  $240r_0$  in the axial direction. The peak of sound emission is respectively found before and after the closure of the potential core for  $Re_D = 12500$  and  $Re_D = 3125$ . Cross-correlations between the flow and acoustic fields show that Mach wave radiation is the dominant noise generation mechanism. Moreover, shock structures similar to those found in the acoustic fields of spatial supersonic jets emitting crackle noise are also observed in the immediate vicinity of the flow. It supports the idea that this distinctive feature of the noise generated by high-speed supersonic jets is mainly the result of a source mechanism located inside the turbulent flow. For both jets, the generation of these steep wavefronts occurs at the times of maximum sound emission. It also appears that shock structures are more frequently detected in the sound field of the jet at  $Re_D = 12500$ , and that they are stronger. A conditional averaging procedure is used to extract generic features of the formation of these shock waves. For the two Reynolds number considered, they appear to be generated by the supersonic motion of coherent structures inside the flow and their generation process thus shows high degrees of similarity with Mach wave radiation. Further

investigations are however needed to understand the influence of the exhaust parameters on the shape of the observed waveforms. Additional numerical simulations of temporally developing jets are underway to investigate the effects of temperature and Mach number on the generated shock structures. Moreover, simulations of spatially-developing jets at comparable exhaust conditions are needed to investigate the resemblance of the shock waves radiated by these low Reynolds number temporal jets with the ones radiated by more realistic spatially-developing jets.

## Acknowledgments

This work was granted access to the HPC resources of FLMSN (Fédération Lyonnaise de Modélisation et Sciences Numériques), partner of EQUIPEX EQUIP@MESO, and of the resources of IDRIS (Institut du Développement et des Ressources en Informatique Scientifique) under the allocation 2016-2a0204 made by GENCI (Grand Equipement National de Calcul Intensif). It was performed within the framework of the Labex CeLyA of Université de Lyon, operated by the French National Research Agency (Grant No. ANR-10-LABX-0060/ANR-11-IDEX-0007).

## References

- <sup>1</sup>Tam, C. K. W., “Supersonic jet noise,” *Annual Rev. F. Mech.*, Vol. 27, No. 1, 1995, pp. 17–43.
- <sup>2</sup>Krothapalli, A., Arakeri, V., and Greska, B., “Mach wave radiation: a review and an extension,” *AIAA Paper 2003-1200*, 2003.
- <sup>3</sup>Lowson, M. V. and Ollerhead, J., “Visualization of noise from cold supersonic jets,” *J. Acoust. Soc. Am.*, Vol. 7, No. 12, 1968.
- <sup>4</sup>Oertel, H., “Mach wave radiation of hot supersonic jets investigated by means of a shock tube and new optical techniques,” *Proceedings of the 12th International Symposium on Shock-Tubes and Waves, Jerusalem*, DTIC Document, 1980.
- <sup>5</sup>Tam, C. K. W., “Mach wave radiation from high-speed jets,” *AIAA J.*, Vol. 47, No. 10, 2009, pp. 2440–2448.
- <sup>6</sup>de Cacqueray, N., Bogey, C., and Bailly, C., “Investigation of a high-Mach-number overexpanded jet using large-eddy simulation,” *AIAA J.*, Vol. 49, No. 10, 2011, pp. 2171–2182.
- <sup>7</sup>Nichols, J. W., Lele, S. K., Ham, F. E., Martens, S., and Spyropoulos, J. T., “Crackle noise in heated supersonic jets,” *J. Eng. Gas Turb. Pow.*, Vol. 135, No. 5, 2013, pp. 051202.
- <sup>8</sup>Oertel, H., “Coherent structures producing Mach waves inside and outside of the supersonic jet,” *Structure of Complex Turbulent Shear Flows. IUTAM Symposium, Marseille.*, DTIC Document, 1980.
- <sup>9</sup>Tam, C. and Burton, D., “Sound generated by instability waves of supersonic flows. Part 2. Axisymmetric jets,” *J. Fluid Mech.*, Vol. 138, 1984, pp. 273–295.
- <sup>10</sup>Troutt, T. and McLaughlin, D., “Experiments on the flow and acoustic properties of a moderate-Reynolds-number supersonic jet,” *J. Fluid Mech.*, Vol. 116, 1982, pp. 123–156.
- <sup>11</sup>Tam, C. K., Chen, P., and Seiner, J., “Relationship between the instability waves and noise of high-speed jets,” *AIAA J.*, Vol. 30, No. 7, 1992, pp. 1747–1752.
- <sup>12</sup>Ffowes Williams, J., Simson, J., and Virchis, V. J., “Crackle: An annoying component of jet noise,” *J. of Fluid Mech.*, Vol. 71, No. 02, 1975, pp. 251–271.
- <sup>13</sup>Laufer, J., Schlinker, R., and Kaplan, R., “Experiments on supersonic jet noise,” *AIAA J.*, Vol. 14, No. 4, 1976, pp. 489–497.
- <sup>14</sup>Gee, K. L., Neilsen, T. B., Downing, J. M., James, M. M., McKinley, R. L., McKinley, R. C., and Wall, A. T., “Near-field shock formation in noise propagation from a high-power jet aircraft,” *J. Acoust. Soc. Am.*, Vol. 133, No. 2, 2013, pp. 88–93.
- <sup>15</sup>McInerney, S., “Launch vehicle acoustics. II-Statistics of the time domain data,” *J. Aircraft*, Vol. 33, No. 3, 1996, pp. 518–523.
- <sup>16</sup>de Cacqueray, N. and Bogey, C., “Noise of an overexpanded Mach 3.3 jet: non-linear propagation effects and correlations with flow,” *Int. J. Aeroacoust.*, Vol. 13, No. 7-8, 2014, pp. 607–632.
- <sup>17</sup>Baars, W. J., Tinney, C. E., Wochner, M. S., and Hamilton, M. F., “On cumulative nonlinear acoustic waveform distortions from high-speed jets,” *J. Fluid Mech.*, Vol. 749, 2014, pp. 331–366.
- <sup>18</sup>Anderson, A. T. and Freund, J. B., “Source mechanism of jet crackle,” *AIAA paper 2012-2251*, 2012.
- <sup>19</sup>Buchta, D. A., Anderson, A. T., and Freund, J. B., “Near-field shock radiated by high-speed free-shear-flow turbulence,” *AIAA paper 2014-3201*, 2014.
- <sup>20</sup>Terakado, D., Nonomura, T., Oyama, A., and Fujii, K., “Mach Number Dependence on Sound Sources in High Mach Number Turbulent Mixing Layers,” *AIAA paper 2016-3015*, 2016.
- <sup>21</sup>Krothapalli, A., Venkatakrisnan, L., and Lourenco, L., “Crackle: a dominant component of supersonic jet mixing noise,” *AIAA Paper 2000-2024*, 2000.
- <sup>22</sup>Petitjean, B., Viswanathan, V., and McLaughlin, D., “Acoustic pressure waveforms measured in high speed jet noise experiencing nonlinear propagation,” *Int. J. Aeroacoust.*, Vol. 5, No. 2, 2006, pp. 193–215.
- <sup>23</sup>Viswanathan, K., “Does a model-scale nozzle emit the same jet noise as a jet engine?” *AIAA J.*, Vol. 46, No. 2, 2008, pp. 336–355.

- <sup>24</sup>Murray, N. and Lyons, G., "On the convection velocity of source events related to supersonic jet crackle," *J. Fluid Mech.*, Vol. 793, 2016, pp. 477–503.
- <sup>25</sup>Sandham, N. and Reynolds, W., "Compressible mixing layer-linear theory and direct simulation," *AIAA J.*, Vol. 28, No. 4, 1990, pp. 618–624.
- <sup>26</sup>Vreman, A. W., Sandham, N. D., and Luo, K. H., "Compressible mixing layer growth rate and turbulence characteristics," *J. Fluid Mech.*, Vol. 320, 1996, pp. 235–258.
- <sup>27</sup>Freund, J. B., Lele, S., and Moin, P., "Compressibility effects in a turbulent annular mixing layer. Part 1. Turbulence and growth rate," *J. Fluid Mech.*, Vol. 421, 2000, pp. 229–267.
- <sup>28</sup>Fortuné, V., Lamballais, E., and Gervais, Y., "Noise radiated by a non-isothermal, temporal mixing layer. Part I: Direct computation and prediction using compressible DNS," *Theor. Comput. Fluid Dyn.*, Vol. 18, No. 1, 2004, pp. 61–81.
- <sup>29</sup>Kleinman, R. and Freund, J., "The sound from mixing layers simulated with different ranges of turbulence scales," *Phys. Fluids*, Vol. 20, No. 10, 2008, pp. 101503.
- <sup>30</sup>Bogey, C., "Direct numerical simulation of a temporally-developing subsonic round jet and its sound field," *AIAA paper No. 2017-0925*, 2017.
- <sup>31</sup>Gaster, M., "The role of spatially growing waves in the theory of hydrodynamic stability," *Prog. Aero. Sc.*, Vol. 6, 1965, pp. 251–270.
- <sup>32</sup>Barre, S., Quine, C., and Dussauge, J., "Compressibility effects on the structure of supersonic mixing layers: experimental results," *J. Fluid Mech.*, Vol. 259, 1994, pp. 47–78.
- <sup>33</sup>Zaman, K., "Effect of initial condition on subsonic jet noise," *AIAA J.*, Vol. 23, No. 9, 1985, pp. 1370–1373.
- <sup>34</sup>Bogey, C. and Bailly, C., "A family of low dispersive and low dissipative explicit schemes for flow and noise computations," *J. Comput. Phys.*, Vol. 194, No. 1, 2004, pp. 194–214.
- <sup>35</sup>Mohseni, K. and Colonius, T., "Numerical treatment of polar coordinate singularities," *J. Comput. Phys.*, Vol. 157, No. 2, 2000, pp. 787–795.
- <sup>36</sup>Bogey, C., de Cacqueray, N., and Bailly, C., "Finite differences for coarse azimuthal discretization and for reduction of effective resolution near origin of cylindrical flow equations," *J. Comput. Phys.*, Vol. 230, No. 4, 2011, pp. 1134–1146.
- <sup>37</sup>Morris, P. J., "The spatial viscous instability of axisymmetric jets," *J. Fluid Mech.*, Vol. 77, No. 03, 1976, pp. 511–529.
- <sup>38</sup>Oertel Sen, H., Seiler, F., and Srujijes, J., *New Explanation of Noise Production by Supersonic Jets with Gas Dredging*, Springer Berlin Heidelberg, Berlin, Heidelberg, 2010, pp. 389–397.
- <sup>39</sup>Panda, J. and Seasholtz, R., "Experimental investigation of density fluctuations in high-speed jets and correlation with generated noise," *J. Fluid Mech.*, Vol. 450, 2002, pp. 97–130.
- <sup>40</sup>Veltin, J., Day, B. J., and McLaughlin, D. K., "Correlation of flowfield and acoustic field measurements in high-speed jets," *AIAA J.*, Vol. 49, No. 1, 2011, pp. 150–163.
- <sup>41</sup>Bogey, C. and Bailly, C., "An analysis of the correlations between the turbulent flow and the sound pressure fields of subsonic jets," *J. Fluid Mech.*, Vol. 583, 2007, pp. 71–97.
- <sup>42</sup>Papamoschou, D. and Bunyajitradulya, A., "Evolution of large eddies in compressible shear layers," *Phys. Fluids*, Vol. 9, No. 3, 1997, pp. 756–765.
- <sup>43</sup>Gee, K. L., Shepherd, M. R., Falco, L. E., Atchley, A. A., Ukeiley, L. S., Jansen, B. J., and Seiner, J. M., "Identification of nonlinear and near-field effects in jet noise using nonlinearity indicators," *AIAA paper*, 2007-3653, pp. 2007.
- <sup>44</sup>Baars, W. J. and Tinney, C. E., "Shock-structures in the acoustic field of a Mach 3 jet with crackle," *J. Sound Vib.*, Vol. 333, No. 12, 2014, pp. 2539–2553.